

Robotic Fastening with a Manual Screwdriver

Ling Tang Yan-Bin Jia
Department of Computer Science
Iowa State University
Ames, IA 50010, USA
ling, jia@iastate.edu

Abstract—The robotic hand is still no match for the human hand on many skills. Manipulation of hand tools, which usually requires sophisticated finger movements and fine controls, not only poses a clear technical challenge but also carries a great potential for enabling the robot to assist humans in a wide range of tasks accomplishable using tools. This paper takes a first step to investigate how a robotic arm mounts a rigidly attached screwdriver onto a screw (pre-mounted in a tapped hole) and then tightens it using the tool. Mounting begins with sliding the screwdriver tip on the screw head along preplanned paths to search for the drive and follows with rotating the screwdriver to drop the tip into the drive. Prevention of a slip off the screw head is achieved via impedance control to install a “virtual fence” along its boundary. Turning of the screw is conducted via hybrid position/admittance control based on modeling the reaction force between the screw and the substrate. Simulation results with a KUKA Arm demonstrate the smoothness of the entire action.

I. INTRODUCTION

Decades of research have made significant progress in robotic grasping [1] and dexterous manipulation [2], [3]. The skill level of robotic hands today is still limited in that many fine manipulation tasks are still beyond their reach. Such a hand is most likely intended for work or assistance in the human environment, where everyday tasks are often configured to be solved using hand tools. Tool usage not only tests the hand’s dexterity and versatility but also serves as a milestone for the achievement of human-level dexterity. It has great potentials in home automation, where the robot can take over many chores, elderly assistance, where health care costs can become more affordable, and medical robotics, where robotic hands capable of maneuvering medical tools can reduce fatigue of doctors and nurses and improve the chance of success in an operation.

Robotic tool usage has been investigated for its different phases from tool recognition [4], [5] to tool grasping and orientation [6], [7], [8], [9], [10]. Despite demonstrations on tasks such as bolt unscrewing [11], drilling [12], plant watering [13], etc., the level of exhibited dexterity has been primitive due to ignorance of friction, compliance, and control. Furthermore, hand tools have been mostly excluded because they require maneuver skills.

Our attention on tool usage turns to fastening [14], which encompasses a broad class of tasks where fasteners such as

screws, bolts, and nuts are used to hold objects together under torquing actions applied by tools such as screwdrivers and wrenches. Fastening is fundamental to industrial assembly and common in household tasks. Power tools such as electric screwdrivers and impact wrenches are fast and suitable for high volume industrial productions. They are, however, also bulky (unable to reach a fastener within a very small space), limited (not to be used in the vicinity of conductive matter such as water), and in need of a setup.

In this paper, we investigate the task of screw driving by a robotic arm using a hand screwdriver with a focus on two maneuvers: insertion of the screwdriver tip into the drive of a screw and torquing of the screw to tightness. This preliminary investigation assumes that the screwdriver is rigidly mounted on the arm and the screw is pre-mounted (but not tightened) into a substrate as shown in Fig. 1. Alignment of two threaded parts before fastening has been investigated based on vision [15], [16] or force and position feedback [17].

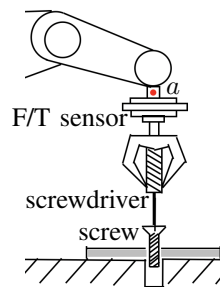


Fig. 1: Task setup.

Insertion of the screwdriver tip can be viewed as a generalized version of the well-studied peg-in-hole problem [18], [19], [20], [21], [22]. Existing results, primarily concerning cylindrical pegs and holes, are not easily adaptable to other shapes. In Section II, we present a strategy that first searches for the drive by moving the tip on the screw head under hybrid control [23] in at most four passes. A virtual wall is installed around the head’s boundary under impedance control [24] to prevent the tip from sliding off the boundary. As soon as the drive is encountered by the sliding tip, the screwdriver is first rotated compliantly against one of its edges until the tip is tangent to the edge, which then initiates a downward movement that will end with the tip in contact with the drive’s bottom. A second rotation then aligns the tip’s edge with the bottom and a third rotation stabilizes the tip inside the drive to get the screwdriver ready for torquing.

The action of fastening has been investigated on modeling or analysis of the fastener-substrate interactions [25], [26], [27], [28], [29] and control of the fastener’s motion [30], [31], [32], [33]. Section III studies arm control to perform screw driving through contacts at the screwdriver tip and between the threads of the screw and the hole in the substrate.

*Support for this research was provided by Iowa State University (ISU). The authors would like to thank Shengwen Xie for his initial effort and thoughts on the problem.

Contact force at the tip is measured by a force/torque sensor connecting the arm’s end-effector and the screwdriver. Contact force between threads can be estimated based on the analysis in [26] and from the current pose of the screwdriver. We describe a hybrid strategy that conducts position/force control along the axial direction to drive the screw forward, and admittance control in the four other directions to keep the screwdriver and screw from deviating too much from the hole’s axis. Section IV shows simulation results on the platform MuJoCo with a KUKA Arm. Section V summarizes the paper with a discussion over future direction.

The contributions of this paper include: 1) a reliable control strategy for tip insertion based on the force/torque feedback; 2) an interaction model that computes the force/torque due to the screw’s penetration into the substrate in linear time; and 3) a hybrid controller for screw driving that integrates position, force, admittance, and null space controls.

II. SCREWDRIVER MOUNTING ONTO SCREW

Pickups of the screwdriver/screw and pre-mounting of the latter by a robotic hand require complicated finger actions and dealing of issues such as cross threading and jamming, all of which are beyond the paper’s scope.

We assume that a screw has been pre-mounted into a threaded hole and is waiting to be tightened by a screwdriver (see 1). The first step is to mount the screwdriver tip inside the screw’s drive. Suppose we have a robotic arm with n degrees of freedom (DOFs). Its end-effector and a screwdriver are rigidly joined together by a 6-DOF force/torque sensor. To operate the screwdriver, $n \geq 6$ must hold. The following assumptions are made:

- The screw remains stable inside the hole.
- Its pose is approximately known.
- Its drive has unknown orientation.

Vision is of limited utility for controlling force in contact-based tasks, and is prone to occlusion¹. The robotic arm’s control inaccuracy further increases the difficulty in operating the screwdriver in such a confined space. Nevertheless, compliance between the screwdriver and the screw can be utilized to carry out the operation with force sensing available.

The action of mounting the screwdriver onto the screw drive is divided into three steps as shown in Fig. 2: (a)–(b) establishing the contact between the screw and the screwdriver, (b)–(c) searching for the screw drive, and (c)–(d) rotating the screwdriver to insert the tip.

A. Touchdown onto the Screw

First, the tip moves down to touch the screw head’s center, whose position is estimated beforehand with some error. During the movement, the screwdriver is tilted about its body y -axis (perpendicular to the shaft plane) for a small angle η (see Fig. 2a). This leads to a point contact with the screw head as shown in Fig. 2b.

¹For a standard slotted machine screw, the diameter of the head ranges from 1 to 25 mm, while the width of the drive ranges from 0.6 to 2.7 mm. The range of noise for a depth-sensing camera can vary from ± 1 to ± 5 cm at a distance of ± 1 m.

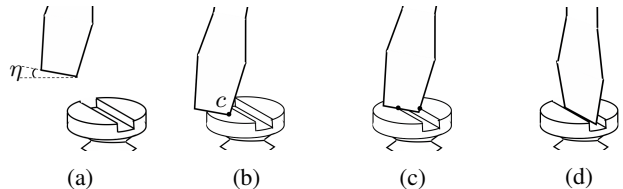


Fig. 2: Four snapshots of tip insertion into the drive: (a) initial configuration, where η is a small tilting angle of the screwdriver; (b) contact establishment at the tip point c and drive search; (c) tip point in the drive; and (d) the screwdriver shank in contact with the drive’s two walls.

Denote θ as the vector of n joint angles, τ as the vector of joint torque, and $\rho_a = (f_x, f_y, f_z, \tau_x, \tau_y, \tau_z)^\top$ as the wrench vector exerted at a reference point a on the arm’s end-effector (see Fig. 1). ρ_a is read by the sensor after compensating the gravitational effects of the sensor and the screwdriver. The arm’s dynamics is described in the joint space as $\tau = M(\theta)\ddot{\theta} + C(\theta, \dot{\theta})\dot{\theta} + N(\theta) - J_a^\top \rho_a$, where $M(\theta)$ is the mass matrix including the screwdriver and F/T sensor, $C(\theta, \dot{\theta})$ is the Coriolis and centrifugal term, $N(\theta)$ is the gravity term, and J_a is the $6 \times n$ Jacobian matrix at the point a .

We define the state variable as $x = (x, y, z, \alpha, \beta, \gamma)^\top$ in the task space, where (x, y, z) represents the position of the tip point c (see Fig. 2b), and (α, β, γ) are the z - y - x Euler angles to describe the screwdriver’s orientation. We have $\dot{x} = J_c \dot{\theta}$ for some Jacobian J_c . Differentiating this velocity equation and substituting it into the arm dynamics in the joint space, we have the dynamics in the task space as $\tau = M J_c^\dagger \ddot{x} + N_c - J_a^\top \rho_a$, where J_c^\dagger is the pseudoinverse of J_c and $N_c = -M J_c^\dagger J_c \ddot{\theta} + C \dot{\theta} + N$.

1) *Descending onto the Screw*: The tip translates along a desired trajectory $x_d(t) \in \mathbb{R}^6$ until it establishes contact with the head. With a rough estimation of the screw’s position, we can set the destination to be slightly below the plane of the head. Let $x_e = x_d - x$ be the pose error. We apply the following proportional-integral-differential (PID) position controller in the world frame $\{w\}$

$$\tau = M J_c^\dagger (\ddot{x}_d + k_v \dot{x}_e + k_p x_e + k_i \int x_e dt) + N_c - J_a^\top \rho_a. \quad (1)$$

It is easy to verify that the resulting error dynamics has asymptotic error convergence.

2) *Contact Softening*: When the tip contacts the head, the F/T sensor readings will increase suddenly because of the impact. To soften it, we switch from position control to impedance control in the contact normal direction. The body frame s of the screw is affixed to the center of the screw tip, with its z -axis aligned with the screw axis that extends towards the head, and its x -axis arbitrarily chosen. Denote $[x]_i$ as the i -th component of the vector x . The control objective is to allow the arm’s behavior in the screw’s axial direction to mimic that of a system with mass m_o , stiffness k_s , and damping k_d . This target compliant behavior is described as

$$m_o [{}^s \ddot{x}_e]_3 + k_d [{}^s \dot{x}_e]_3 + k_s [{}^s x_e]_3 = -[{}^s \rho_a]_3, \quad (2)$$

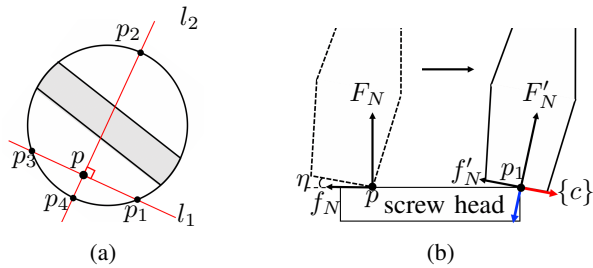


Fig. 3: Search for the drive: (a) sliding paths l_1 and l_2 for the tip; (b) tip sliding on the head along $\overrightarrow{pp_1}$ to reach an edge. The moving direction agrees with the tip's tilting direction.

where $[\mathbf{x}_e]_3 = [\mathbf{x}_o]_3 - [\mathbf{x}]_3$ represents the z -directional position displacement of the frame $\{s\}$, and $[\mathbf{x}_o]_3$ is the equilibrium position of $[\mathbf{x}]_3$ in the absence of the normal force $[\mathbf{s}\rho_a]_3$. Here, $[\mathbf{x}_o]_3$ is set to be slightly below the head's plane to maintain the contact throughout the process.

Under the assumption that the screw is not moving, we have $\ddot{\mathbf{x}} = \tilde{R}^\top \mathbf{s}\ddot{\mathbf{x}}$, where $\tilde{R} = \text{diag}(R, R)$ with R being the rotation matrix from the world frame to $\{s\}$. Substituting this into the arm dynamics, we represent the dynamics in the screw frame:

$$\boldsymbol{\tau} = M J_c^\dagger \tilde{R}^\top \mathbf{s}\ddot{\mathbf{x}} + \mathbf{N}_c - J_a^\top \tilde{R}^\top \mathbf{s}\rho_a. \quad (3)$$

For the other components of $\mathbf{s}\ddot{\mathbf{x}}$ (except $[\mathbf{s}\ddot{\mathbf{x}}]_3$), we apply similar position control as in (1), except that now all the variables are in the screw frame $\{s\}$. We get a hybrid position-impedance controller for softening the contact by plugging the PID servo from (1) into (3), and replacing $[\mathbf{s}\ddot{\mathbf{x}}]_3$ with $[\mathbf{s}\ddot{\mathbf{x}}]_3 + (k_d[\mathbf{s}\dot{\mathbf{x}}]_3 + k_s[\mathbf{s}\mathbf{x}_e]_3 + [\mathbf{s}\rho_a]_3)/m_o$ from (2).

B. Searching for the Screw Drive

In a most likely scenario, the tip point c does not go inside the screw's drive directly when it lands on the head. Our next step is to search for the drive by sliding the tip on the surface of the head. Here we describe a search strategy² that uses two orthogonal sliding paths on the head.

1) *Drive Search*: We let the tilted tip slide on the head while maintaining a stable normal force. When the tip reaches an edge of either the drive or the head's boundary, a sudden change in the force between the tip and the head is captured by the sensor because of the sudden change in the frictional force (see Fig. 3b). The choice of the tilting angle, η , depends on the sensitivity of the sensors.

Let p be the initial contact point of the tip and the head, and l_1 be the line that is parallel to the projection of the tip's bottom edge onto the head's plane. The line l_2 is in the same plane but perpendicular to l_1 at p . As shown in Fig. 3a, l_1 intersects the head boundary at p_1 in the direction that the tip tilts to, and the two lines intersect the boundary at four points (p_1, p_2, p_3 and p_4) in the counterclockwise order.

The tip first slides along $\overrightarrow{pp_1}$ until it encounters the drive or reaches the head's boundary. If no drive is discovered, the tip reverses its sliding direction along l_1 , and moves back to p . It

then rotates counterclockwise through $\pi/2$ to align the tilting direction with $\overrightarrow{pp_2}$, followed by a tip sliding in the same direction. In the worst case, the drive search is performed in four directions as $\overrightarrow{pp_1}$, $\overrightarrow{pp_2}$, $\overrightarrow{pp_3}$, and $\overrightarrow{pp_4}$, sequentially.

Sliding is carried out under hybrid position/force control in the screw frame $\{s\}$, which uses the dynamics from (3). We use PID control over the pose of the screwdriver with a replacement of $[\mathbf{s}\ddot{\mathbf{x}}]_3 = 0$, which is ensured because the tip is moving on the surface of the head. Force control in the z -direction is realized by replacing the normal force component of $\mathbf{s}\rho_a$ in (3) with a servo $f_d + k_i \int f_e dt$, where $f_e = f_d - f_z$ with f_d being some desired force and f_z being the actual normal force detected by the sensor.

2) *Prevention of Sliding off the Screw Head*: Tip sliding ends in one of two situations: i) it reaches one of the straight edges bounding the drive; and ii) it reaches the circular boundary of the head (see Fig. 3b). In both situations, the contact will experience a sudden change to be captured by the F/T sensor at the end-effector.

When an edge e is encountered, it is important to stabilize the tip (and the screwdriver) instantly. At the instant, the contact between the tip point and the head immediately switches to one between the edge e and the tip's bottom edge. This allows time to stop the tip's movement and prevent the tip from sliding off the edge.

Control is done in the frame $\{c\}$ attached to the screw at its boundary intersection with the tip edge (see Fig. 3b), such that its x - and z -axes are aligned with the tip edge and the screwdriver axis, respectively. The arm dynamics in this frame is similar to (3) with the replacements of the frame superscripts $\{s\}$ by $\{c\}$. We use impedance control to stop the sliding by implementing the compliant behavior in (2) with the translational components (i.e., x , y , and z) of ${}^c\mathbf{x}$, as if a virtual wall is installed along the edge e . Meanwhile, the screwdriver's orientation, represented by the Euler angles, is placed under position control.

3) *Edge Discrimination*: We cannot distinguish a drive edge from the head boundary by the change in force solely, because the relative orientation between the tip and the screw is unknown. Therefore, a simple test is conducted by letting the tip continue to slide along its bottom edge (see Fig. 3b). If it has encountered a drive edge, there will be a second change in the force direction when the tip contacts the opposite edge of the drive. If there is no such change within a distance of δ (determined by its tilting angle and the drive width), the tip has reached the head's boundary.

To realize the above movement, we can switch the impedance control in the x -direction of the frame $\{c\}$ to position control with a desired constant velocity. The remaining five directions are placed under the same control applied to stabilize the tip at an edge during the drive search earlier.

C. Tip Insertion

Once the tip is inside the drive with contacts established at both edges of the drive, it needs to be fully inserted before fastening. We carry out this insertion in a sequence of three rotations to be described below.

²The initial idea was conceived by Shengwen Xie.

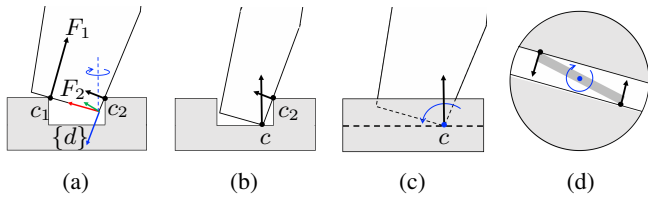


Fig. 4: Tip insertion: (a) rotation about an axis that is perpendicular to the head while maintaining the two contact points c_1 and c_2 ; (b) disappearance of the contact at c_1 causing a fall of the tip inside the drive; (c) rotation to align the axis of the screwdriver with that of the screw; (d) rotation about the screwdriver's axis to reach the configuration before torquing.

First, the screwdriver rotates about an axis that is perpendicular to the screw head and passes through the tip point. The control is performed in an instantaneous frame $\{d\}$ at the current tip point and in the same orientation as the screwdriver (see Fig. 4a). Meanwhile, it maintains two contacts, c_1 and c_2 , with the two drive edges. We use simple PID servos for controlling the orientation of the screwdriver. In the x -direction, we still employ impedance control, except that now the equilibrium point is set on the x -axis slightly into the drive edge in order to maintain the contact at c_2 with a small force F_2 . In the z -direction, a constant force F_1 is maintained at c_1 such that $|F_1| \gg |F_2|$. When the contact at c_1 disappears during the rotation, a change of force can be detected by the sensor, showing that the entire tip is inside the drive. At this moment, the frictional force at c_2 will be unable to counter the force applied by the robot in the z -direction. Consequently, the tip will drop into the drive (Fig. 4b), generating an impact that can be softened via impedance control in the screw's axial direction.

After the drop, the tip may not be centered in the drive. So, we let the tip slide inside the drive in one direction until it detects the boundary of the head (as described in the drive search). Subsequently, the tip can be centered in the drive by utilizing the drive boundary and the diameter of the screw head. Now, a second rotation of the screwdriver is performed until its axis aligns parallel to the screw axis (see Fig. 4c), along which a constant contact force is maintained. An axial rotation is then performed until a torque is sensed in the axial direction. At this point, the screwdriver is well-positioned and ready to drive the screw.

III. SCREW DRIVING

The next step is to control the mounted screwdriver to drive the screw. Enough friction can be generated to prevent the screwdriver tip from sliding in the drive, by exerting a moment in the screw's axial direction via the screwdriver.

A. Modeling Force/Torque on the Screw from the Substrate

To conduct simulation, we need an interaction model between the screw and the threaded hole. This comes down to computation of the force and torque received by the screw due to its penetration into the hole. Such modeling is also necessary in the future work, where the screwdriver is held

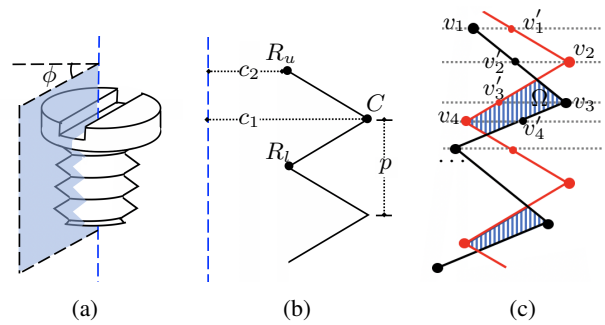


Fig. 5: Modeling the screw-hole interaction: (a) a cross section within a plane through the screw axis; (b) triangular element $\triangle R_u C R_l$ in the cross section of the screw; and (c) its penetration into a cross section of the hole represented by the red polyline.

by a robotic hand and the dynamics of the screwdriver is considered separately.

Consider the screw thread as the trajectory of a triangular element (see Fig. 5b) rotating and translating along the screw axis simultaneously. The three vertices of this triangle move along separate helices: the crest curve $c(\phi) = (c_1 \cos \phi, -c_1 \sin \phi, \frac{\phi}{2\pi} p)^\top$, and the upper/lower root curves $r_{u/l}(\phi) = (c_2 \cos \phi, -c_2 \sin \phi, \frac{\phi}{2\pi} p \pm \frac{p}{2})^\top$, where ϕ gives the amount of the rotation along the helix, c_1 is the major radius (distance from the crest to the screw/hole axis), c_2 is the minor radius (distance from the root), and p denotes the pitch.

Let $\{s\}$ be the screw frame as introduced in II-A.2, except that now, with the drive orientation known from forward kinematics, its x -axis points to the starting point of the thread. We set the hole frame $\{h\}$ at the center of the hole's plane, with its z -axis pointing into the hole, and x -axis similarly defined as for $\{s\}$. We can easily calculate the coordinates of the three points in each thread element from the above helix functions for both frames.

Figure 5c illustrates the thread engagement between the screw and the hole in the plane through the screw axis as determined by the angle ϕ . We can calculate all the vertices on the hole's thread within the cross section by plugging $\phi + 2i\pi$ ($i = 0, 1, 2, \dots$) into the functions $c(\phi)$ and $r_{u/l}(\phi)$. Because of the slight tilting of the screw, the plane containing the axial cross section at ϕ of the screw may not coincide with the hole's plane at the same angle. However, this error is small enough to be ignored. We use the same functions to get the vertices on the screw threads, and transform the coordinates in $\{s\}$ into $\{h\}$ by their relative pose.

As shown in Fig. 5c, the intersections of the screw thread and the hole thread in the same plane appear at most once between the vertices. Therefore, with all the vertices known, we can do a plane sweep [36] to calculate the penetration area efficiently. As we walk along the vertices on both threads from top to bottom, it is easy to check if the screw penetrates into the wall or not at each vertex v_i by comparing it with the point on the other thread at the same height (Fig. 5c). This check is discussed in detail in [35].

Between two adjacent vertices, three cases may arise: i) the screw penetrates into the wall at v_i but not at v_{i+1} , which indicates an intersection happening in between; ii) the screw penetrates at v_i but not at v_{i+1} , which suggests the end of the intersection; and iii) both v_i and v_{i+1} have the same condition, which implies that there is no change of the intersection status. With all the vertices of the penetration region Ω known, we can calculate its area A trivially. This allows us to estimate the force based on the area using a simple spring model $F = kA$, where k is a stiffness constant, and apply the force at the center of Ω in a direction normal to its upper or bottom edge (depending on the center of Ω). With all the normal forces determined along the threads, the frictional forces and the torques can be determined. Finally, we integrate all the forces and torques for all cross sections over $\phi = [0, 2\pi)$ to get the force and torque exerted on the screw by the threads in the hole. This computation can be done in linear time regarding the number of threads engaged between the screw and the hole.

B. Hybrid Control for Torquing

The screw moves a distance of $\Delta d = (p \times \Delta\theta)/2\pi$ along the hole's axis, where $\Delta\theta$ is the amount of the screw's rotation about the hole's axis. This implies a redundancy in the state variable x . Differentiating the equation above and representing it in terms of the state variable x , we get ${}^h\dot{x}_3 = \frac{p}{2\pi} [{}^h\omega]_3$ where ${}^h\omega \in \mathbb{R}^3$ is the angular velocity of the screw in the hole frame $\{h\}$. Denote a new state variable as $\zeta = [{}^h x, {}^h y, {}^h \alpha, {}^h \beta, {}^h \gamma]^\top$. Here, ${}^h x$ and ${}^h y$ give the tangential displacements between the centers of the head and the hole in the frame $\{h\}$, and $({}^h \alpha, {}^h \beta, {}^h \gamma)$ are the z - y - x Euler angles of the screw frame $\{s\}$ relative to the hole frame $\{h\}$. From the relationship between ${}^h\dot{x}_3$ and ${}^h\omega_3$, we get the screw's velocity as

$${}^h v = \begin{bmatrix} 1 & 0 & 0 & 0 & 0 \\ 0 & 1 & 0 & 0 & 0 \\ 0 & 0 & 0 & 0 & p/2\pi \\ 0 & 0 & 1 & 0 & 0 \\ 0 & 0 & 0 & 1 & 0 \\ 0 & 0 & 0 & 0 & 1 \end{bmatrix} \begin{bmatrix} I_2 & \mathbf{0} \\ \mathbf{0} & S \end{bmatrix} \dot{\zeta}, \quad (4)$$

where S is a matrix that transforms Euler angle rates to the angular velocity. We let Σ and T denote the first two matrices on the right hand side of the above equation. It follows from the arm kinematics that ${}^h v = J_h \dot{\theta}$, where ${}^h v = [{}^h v_p, {}^h v_r]^\top$ gives the translational and angular velocities in the frame $\{h\}$, and J_h is a Jacobian matrix. From (4), we obtain $\zeta = T^{-1} \Sigma^\dagger J_h \dot{\theta}$. Differentiating this equation, and substituting the result into the arm dynamics in the frame $\{h\}$, we get the dynamics expressed in the task coordinates ζ .

For the rotation about the hole's axis, we simply use position control to track a desired trajectory specified by the rotation angle as a function of time, say $\theta(t) = [\omega_d]_3 t$, where $\omega_d = [0, 0, \dot{\theta}]^\top$ is the desired angular velocity. For translational and rotational movements in the tangential directions (i.e., four directions represented by ${}^h p = [{}^h x, {}^h y, {}^h \alpha, {}^h \beta]^\top$),

we use the modeled force/torque components to keep the screw axis from any sizable deviation from the hole's. This is realized via admittance control to make the robot yield to the force/torque with a movement in each corresponding direction. The target compliant behavior is $M_o({}^h \ddot{p}_d - {}^h \ddot{p}) + K_d({}^h \dot{p}_d - {}^h \dot{p}) + K_s({}^h p_d - {}^h p) = -{}^h f$, where ${}^h f$ is the combined force and torque in the tangential directions of ρ_a . From the above equation, we solve for ${}^h \ddot{p}_d$. The desired trajectories ${}^h \dot{p}_d$ and ${}^h p_d$, obtained through integration of ${}^h \ddot{p}_d$, are then used for position control in the task space within the frame $\{h\}$.

Besides the control over the state variable ζ , we also need to maintain a force in the axial direction of the hole to prevent the tip from slipping out of the drive or the screw's threads from being damaged.

C. Joint Limit Prevention via Null Space Control

The process of screw driving (tip insertion as well) involves large amount of rotations that may exceed the reach of a robotic arm. Although a 6-DOF arm sufficient for the task, the range of the screw positions it can operate on may be very constrained. This limitation can be alleviated if extra degrees of freedom is available. In such cases, null space control can shift the load between joints, thereby reducing the chance of a joint limit being exceeded.

The null space of the Jacobian J_a at the end-effector characterizes all the joint motions that have no effect on the screw driving task (as the screwdriver is rigidly attached). An artificial potential field function [34] can be constructed as $V(\theta) = k \sum_{i=1}^n \left([\theta]_i - \frac{[\theta_{\min}]_i + [\theta_{\max}]_i}{2} \right)^2$, where θ is the vector of joint angles, θ_{\min} and θ_{\max} represent the lower and upper joint limits, respectively. We can add an extra term $\tau_{\text{null}} = -(I_n - J_a^\dagger J_a) \nabla V(\theta)$ to our controller. It will guide the joint movement in the null space of J_a with the tendency to minimize $V(\theta)$, which helps to keep every joint angle $[\theta]_i$ in the middle of its range.

IV. SIMULATION

The simulations are conducted on the platform MuJoCo with a 7-DOF KUKA LBR iiwa robot. The setup³ is shown in Fig. 6a. This section first presents a successful execution of screwdriver mounting and screw driving, and then summarizes over all executions.

A. Sequential Executions of Mounting and Torquing

Mounting starts with the screwdriver moving down to establish a point-surface contact with the head (Fig. 6b). Then (b)–(g) show a drive search as described in II-B.1, while keeping the normal force of the contact frame within 1 ± 0.03 N. Fig. 7 shows the insertion of the tip. During the first rotation in (a)–(b), the employed hybrid controller

³The screw parameters include: 1) pitch $p = 1.30$ mm; 2) drive width $w = 2.00$ mm; 3) major radius $c_1 = 0.50$ mm; and 4) minor radius $c_2 = 0.38$ mm. The hole parameters are scaled according to the screw's with 1.07. The control parameters include: 1) $K_p = 400$, $K_v = 35$, $K_i = 500$ (position control); 2) $k_i = 0.5$ (force control); 3) $m_o = 10$, $k_d = 200$, $k_s = 50$ (impedance control); and 4) $M_o = 10$, $K_d = 4000$, $K_s = 100$ (admittance control).

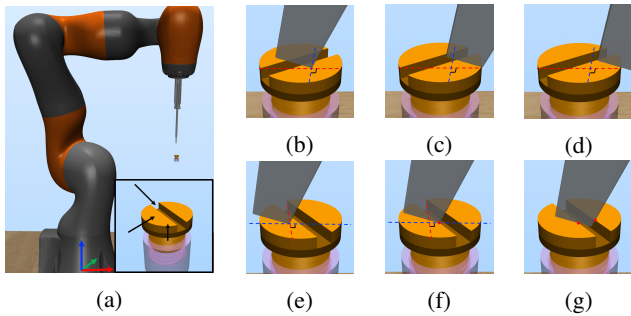


Fig. 6: Search for the screw drive: (a) simulation setup; (b) touchdown to the head with a tip tilting angle of $\pi/10$; (c) end of the search along the line l_1 (red) at the boundary with a force direction change in 0.2115 rad detected by the sensor; (d) sliding along the tip edge that classifies it as the head boundary with consistent force readings; (e)–(g) changed search direction along the orthogonal line l_2 (blue) that finds the drive as described in II-B.1.

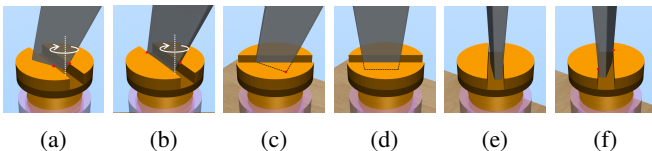


Fig. 7: Tip insertion involves three rotations about: (a)–(b) an axis that is perpendicular to the screw head and passes through the tip point; (c)–(d) the direction perpendicular to the shaft; and (e)–(f) the screwdriver’s axis.

maintains a contact force (2 ± 0.05 N) at c_1 in the negative z -direction, and a contact force (0.5 ± 0.1 N) at c_2 in the positive x -direction (cf. Fig. 4a). A torque of 0.01 Nm in the screwdriver’s axial direction is sensed when the final configuration in (f) is reached. During the last two rotations, a force in the range 1 ± 0.03 N along the normal direction of the contact frame is maintained to prevent contact loss.

The initial configuration in Fig. 8a for torquing is the same as that in Fig. 7f. The robot configuration is reset in (c) by rotating the screwdriver counterclockwise through π . With the drive’s orientation known before the disengagement, the tip is easily inserted back to begin the next round. The normal force to the screw head is maintained within 5 ± 0.02 N, while the torque increases from 0.0107 Nm in (a) to 0.0145 Nm in (d). Meanwhile, impedance control applied in the orthogonal directions will keep the force within the range ± 0.03 N.

B. Results

For further testing, we conducted forty simulation trials. Each trial randomly selects the position of the screw in a 0.05 m box centered at (0.3, 0.0, 0.4) m, and the direction of the drive from $[0, 2\pi)$. All the twenty trials on mounting can identify the drive, but only fifteen of them end up with successful tip insertions. Five trials fail because a joint of the arm has reached its limit to inhibit the robot from completing a specific rotation. It is possible to avoid such failures by a different initial configuration or a better motion planning. Among the successful trials, the time for mounting task varies from 50 to 110 seconds, as affected by the drive search. For screw driving, all the twenty trials have seen

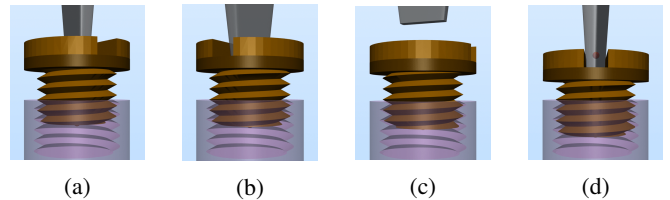


Fig. 8: Screw driving: (a) initial configuration; (b) clockwise rotation through $\pi/3$; (c) disengagement of the screwdriver when reaches the joint limits after a torquing through $4\pi/5$; and (d) configuration after two iterations.

the completion of three iterations of the following steps: torquing, disengagement, joint reset, and insertion again. The average time for a complete iteration is 15 seconds.

It is worth mentioning that when null space control is not activated, most of the trials would fail easily on a rotation. For example, during torquing, there is a tendency to use only the first six joints of a 7-DOF KUKA robot instead of the last joint whose axis coincides with the screwdriver.

V. DISCUSSION AND FUTURE WORK

This paper presents control policies for mounting a screwdriver and using it to tighten a screw. The mounting strategy solves a generalized peg-in-hole problem by combining a sliding-based search for the screw drive with controlled rotations that utilize compliance for tool tip alignment and insertion. Installation of the virtual fence around the screw’s head carries a good promise for mating of small parts. The tightening strategy maintains the axial alignment of the screw and the threaded hole based on modeling and regulating their interactions. Various control policies, over position, impedance, and admittance, are integrated smoothly to execute this fine manipulation task. The proposed mounting strategy can be adapted to a Phillips screw, because the tip of the matching screwdriver can be treated as a point. On the other hand, for a hex drive screw, mounting the screwdriver tip can be more challenging as it requires perfect alignment between the tip and the drive. The torquing strategy works for various types of screws as long as the screwdriver tip does not slide in the drive.

The work needs to be extended in several directions to approach the skill level of screw driving by the human hand. Clearly, the screwdriver should be held and maneuvered by a robotic hand (mounted on a robotic arm). This leads to issues of tool pickup, maneuver, and exchange, all of which rely on executions of finger gaits involving contact establishment, maintenance, and disengagement. Impedances between the fingertips and the screwdriver and between the screwdriver and the screw will serve an important role during the fastening action. Effective finger and screwdriver control policies will require more accurate modeling of the screw-substrate contact force, which cannot be sensed directly. Other tasks, such as retrieving and pre-installing a screw into a threaded hole by a robotic hand, also present challenges.

REFERENCES

- [1] Antonio Bicchi and Vijay Kumar. Robotic grasping and contact: A review. In *Proc. IEEE Int. Conf. Robot. Autom.*, 2000, pp. 348–353.
- [2] Antonio Bicchi. Hands for dexterous manipulation and robust grasping: a difficult road toward simplicity. *IEEE Trans. Robot. Autom.*, vol. 16, no. 6, pp. 652–662, 2000.
- [3] A. M. Okamura, N. Smaby, and M. R. Cutkosky. An overview of dexterous manipulation. In *Proc. IEEE Int. Conf. Robot. Autom.*, 2000, pp. 255–262.
- [4] Ingo Kresse, Ulrich Klank, and Michael Beetz. Multimodal autonomous tool analyses and appropriate application. In *IEEE-RAS Int. Conf. Humanoid Robots*, 2011, pp. 698–613.
- [5] V. Tikhonoff, U. Pattacini, L. Natale, and G. Metta. Exploring affordances and tool use on the iCub. In *IEEE-RAS Int. Conf. Humanoid Robots*, 2013, pp. 130–137.
- [6] S. Gupta, C. J. Paredis, and P. Brown. Micro planning for mechanical assembly operations. In *Proc. IEEE Int. Conf. Robot. Autom.*, 1998, pp. 239–246.
- [7] M. Toussaint, K. Allen, K. A. Smith, and J. B. Tenenbaum. Differentiable physics and stable modes for tool-use and manipulation planning. In *Robot. Sci. Syst.*, 2018.
- [8] Wenbin Li and Mario Fritz. Teaching robots the use of human tools from demonstration with non-dexterous end-effectors. In *IEEE-RAS Int. Conf. Humanoid Robots*, 2015, pp. 547–553.
- [9] N. Saito, K. Kim, S. Murata, T. Ogata, and S. Sugano. Tool-use model considering tool selection by a robot using deep learning. In *IEEE-RAS Int. Conf. Humanoid Robots*, 2018, pp. 270–276.
- [10] K. Fang, Y. Zhu, A. Garg, A. Kurenkov, V. Mehta, Li Fei-Fei, and S. Savarese. Learning task-oriented grasping for tool manipulation from simulated self-supervision. *Int. J. Robot. Res.*, vol. 39, no. 2–3, pp. 202–216, 2020.
- [11] Tsutomu Hasegawa, Takashi Suehiro, and Kunikatsu Takase. A model-based manipulation system with skill-based execution. *IEEE Trans. Robot. Autom.*, vol. 8, no. 5, pp. 535–544, 1992.
- [12] Heiko Hoffmann, Zhichao Chen, Darren Earl, Derek Mitchell, Behnam Salemi, and Jivko Sinaopv. Adaptive robotic tool use under variable grasps. *Robot. Autom. Syst.*, vol. 62, pp. 833–846, 2014.
- [13] Jörg Stückler and Sven Behnke. Adaptive tool-use strategies for anthropomorphic service robots. In *IEEE-RAS Int. Conf. Humanoid Robots*, 2014, pp. 755–760.
- [14] Zhenzhong Jia, Ankit Bhatia, Reuben M. Aronson, David Bourne, and Matthew T. Mason. A survey of automated threaded fastening. *Trans. Autom. Sci. Eng.*, vol. 16, no. 1, pp. 298–310, 2019.
- [15] Bruno Lara, Kaspar Althoefer, and Lakmal D. Seneviratne. Automated robot-based screw insertion system. In *Proc. 24th Annu. Conf. IEEE Ind. Electron. Soc.*, 1998, pp. 2440–2445.
- [16] S. Pitipong, P. Pornjit, and P. Watcharin. An automated four-DOF robot screw fastening using visual servo. In *Proc. IEEE/SICE Int. Symp. Syst. Integr.*, pp. 379–383, 2010.
- [17] M. A. Diftler and Ian D. Walker. Experiments in aligning threaded parts using a robot hand. *IEEE Trans. Robot. Autom.*, vol. 15, no. 5, pp. 858–868, 1999.
- [18] D. E. Whitney. Quasi-static assembly of compliantly supported rigid parts. *ASME J. Dynam. Syst. Meas. Control*, vol. 104, pp. 65–76, 1982.
- [19] H. Bruyninckx, S. Dutre, and J. De Schutter. Peg-on-hole: a model based solution to peg and hole alignment. In *Proc. IEEE Int. Conf. Robot. Autom.*, 1995, pp. 1919–1924.
- [20] J. F. Broenink and M. L. Tiernego. Peg-in-hole assembly using impedance control with a 6-DOF robot. In *Proc. 8th Eur. Simul. Symp.*, 1996, pp. 504–508.
- [21] Te Tang, Hsien-Chung Lin, Yu Zhao, Wenjie Chen, and Masayoshi Tomizuka. Autonomous alignment of peg and hole by force/torque measurement for robotic assembly. In *Proc. IEEE Int. Conf. Autom. Sci. Eng.*, 2016, pp. 162–167.
- [22] H. Park, J. Park, D.-H. Lee, J.-H. Park, M.-H. Baeg, and J.-H. Bae. Compliance-based robotic peg-in-hole assembly strategy without force feedback. *IEEE Trans. Ind. Electron.*, vol. 64, no. 8, pp. 6299–6309, 2017.
- [23] M. Raibert and J. Craig. Hybrid position/force control of manipulators. *ASME J. Dynam. Syst. Meas. Control*, vol. 103, no. 2, pp. 126–133, 1981.
- [24] Neville Hogan. Impedance control: An approach to manipulation: Parts I — III. *ASME J. Dynam. Syst. Meas. Control*, vol. 107, pp. 1–24, 1985.
- [25] Edward J. Nicolson and Ronald S. Fearing. Dynamic modeling of a part mating problem: Threaded fastener insertion. In *Proc. IEEE/RSJ Int. Conf. Intell. Robots Syst.*, 1991, pp. 30–37.
- [26] L. Seneviratne, F. Ngemoh, and S. Earles. Theoretical modeling of screw tightening operations. In *Proc. ASME Eur. Joint Conf. Syst. Des. Anal.*, 1992, pp. 189–192.
- [27] L. Seneviratne, F. Ngemoh, S. Earles, and K. A. Althoefer. Theoretical modeling of the self-tapping screw fastening process. *J. Mech. Eng. Sci.*, vol. 215, no. 2, pp. 135–154, 2001.
- [28] Stephen Wiedmann and Bob Sturges. Spatial kinematic analysis of threaded fastener assembly. *ASME J. Mech. Des.*, vol. 128, pp. 116–127, 2006.
- [29] Stephen Wiedmann and Bob Sturges. A full kinematic model of thread-starting for assembly automation analysis. *ASME J. Mech. Des.*, vol. 128, no. 128–136, 2006.
- [30] Takeshi Tsujimura and Tetsuro Yabuta. Adaptive force control of screwdriving with a positioning-controlled manipulator. *Robot. Autom. Syst.*, vol. 7, pp. 57–65, 1991.
- [31] Edward J. Nicolson and Ronald S. Fearing. Compliant control of threaded fastener insertion. In *Proc. IEEE Int. Conf. Robot. Autom.*, 1993, pp. 484–490.
- [32] N. Dhayagude, Z. Gao, and F. Mrad. Fuzzy logic control of automated screw fastening. *Robot. Comput.-Integr. Manuf.*, vol. 12, no. 3, pp. 235–242, 1996.
- [33] Kai Pfeiffer, Adrien Escande, and Abderrahmane Kheddar. Nut fastening with a humanoid robot. In *Proc. IEEE/RSJ Int. Conf. Intell. Robots Syst.*, 2017, pp. 6141–6148.
- [34] Oussama Khatib. Inertial properties in robotic manipulation: An object-level framework. *Int. J. Robot. Res.*, vol. 14, no. 4, pp. 19–36, 1995.
- [35] E. J. Nicolson and R. S. Fearing. Dynamic modeling of a part mating problem: threaded fastener insertion. *Int. Conf. Intell. Robots Syst.*, 1991, pp. 30–37.
- [36] M. de Berg, O. Cheong, M. van Kreveld, and M. Overmars. Computational Geometry: Algorithms and Applications (3rd edition). *Springer-Verlag*, 2008, pp. 20–29.